The Astronomical Journal, 151:96 (13pp), 2016 April doi:10.3847/0004-6256/151/4/96
© 2016. The American Astronomical Society. All rights reserved.

DISCOVERY OF AN ULTRA-DIFFUSE GALAXY IN THE PISCES-PERSEUS SUPERCLUSTER

David Martínez-Delgado[1,2], Ronald Läsker[2], Margarita Sharina[3], Elisa Toloba[4,5], Jürgen Fliri[6,7], Rachael Beaton[5], David Valls-Gabaud[8,18], Igor D. Karachentsev[3], Taylor S. Chonis[9], Eva K. Grebel[1], Duncan A. Forbes[10], Aaron J. Romanowsky[4,11], J. Gallego-Laborda[12], Karel Teuwen[13], M. A. Gómez-Flechoso[14], Jie Wang[15,16], Puragra Guhathakurta[4], Serafim Kaisin[3], and Nhung Ho[17]

[1] Astronomisches Rechen-Institut, Zentrum für Astronomie der Universität Heidelberg, Mönchhofstr. 12–14, D-69120 Heidelberg, Germany
[2] Max-Planck-Institut für Astronomie, Königstuhl 17, D-69117 Heidelberg, Germany
[3] Special Astrophysical Observatory, Russian Academy of Sciences, Russia
[4] University of California Observatories, 1156 High Street, Santa Cruz, CA 95064, USA
[5] The Observatories of the Carnegie Institutions for Science, 813 Santa Barbara Street, Pasadena, CA 91101 USA
[6] Instituto de Astrofísica de Canarias, Vía Láctea s/n, E-38200 La Laguna, Tenerife, Spain
[7] Universidad de La Laguna, Departamento de Astrofísica, E-38206 La Laguna, Tenerife, Spain
[8] LERMA, CNRS UMR 8112, Observatoire de Paris, 61 Avenue de l'Observatoire, F-75014 Paris, France
[9] Department of Astronomy, University of Texas at Austin, 2515 Speedway, Stop C1400, Austin, TX 78712, USA
[10] Center for Astrophysics and Supercomputing, Swinburne University, Hawthorn VIC 3122, Australia
[11] Department of Physics and Astronomy, San José State University, One Washington Square, San Jose, CA 95192, USA
[12] Fosca Nit Observatory, Montsec Astronomical Park, Ager, Spain
[13] Remote Observatories Southern Alpes, Verclause, France
[14] Departamento de Matemática Aplicada (Biomatemática), Universidad Complutense de Madrid, E-28040 Madrid, Spain
[15] National Astronomical Observatories, Chinese Academy of Sciences, Beijing, 100012 China
[16] Institute for Computational Cosmology, Department of Physics, Durham University, South Road, Durham DH1 3LE, UK
[17] Astronomy Department, Yale University, New Haven, CT 06520, USA
[18] Institute of Astronomy, Madingley Road, Cambridge CB3 0HA, UK

Received 2014 March 5; accepted 2016 January 20; published 2016 March 24

ABSTRACT

We report the discovery of DGSAT I, an ultra-diffuse, quenched galaxy located 10°.4 in projection from the Andromeda galaxy (M31). This low-surface brightness galaxy ($\mu_V = 24.8$ mag arcsec^{-2}), found with a small amateur telescope, appears unresolved in sub-arcsecond archival Subaru/Suprime-Cam images, and hence has been missed by optical surveys relying on resolved star counts, in spite of its relatively large effective radius ($R_e(V) = 12''$) and proximity (15′) to the well-known dwarf spheroidal galaxy And II. Its red color ($V - I = 1.0$), shallow Sérsic index ($n_V = 0.68$), and the absence of detectable Hα emission are typical properties of dwarf spheroidal galaxies and suggest that it is mainly composed of old stars. Initially interpreted as an interesting case of an isolated dwarf spheroidal galaxy in the local universe, our radial velocity measurement obtained with the BTA 6 m telescope ($V_h = 5450 \pm 40$ km s^{-1}) shows that this system is an M31-background galaxy associated with the filament of the Pisces-Perseus supercluster. At the distance of this cluster (∼78 Mpc), DGSAT I would have an $R_e \sim 4.7$ kpc and $M_V \sim -16.3$. Its properties resemble those of the ultra-diffuse galaxies (UDGs) recently discovered in the Coma cluster. DGSAT I is the first case of these rare UDGs found in this galaxy cluster. Unlike the UDGs associated with the Coma and Virgo clusters, DGSAT I is found in a much lower density environment, which provides a fresh constraint on the formation mechanisms for this intriguing class of galaxy.

Key words: galaxies: clusters: general – galaxies: evolution – galaxies: formation – galaxies: photometry

1. INTRODUCTION

Small aperture (10–15 cm) telephoto-lens telescopes, combined with the new generation of commercial CCD cameras, can be valuable instruments to search for low-surface-brightness stellar systems, such as new dwarf companions (Merritt et al. 2014; Javanmardi et al. 2015; Karachentsev et al. 2015; Romanowsky et al. 2016) and stellar tidal streams (Martínez-Delgado et al. 2008, 2010) around nearby spiral galaxies, and ultra-diffuse galaxies (UDGs) in galaxy clusters (van Dokkum et al. 2015a). The short focal ratio of these telescopes allows one to trace these faint stellar systems as unresolved, diffuse light structures with surface brightness below $\mu_V = 25.5$ mag arcsec^{-2} well beyond the Local Group, up to distances of ∼50–100 Mpc, exploring the low-surface-brightness regime of the scaling relations for early-type galaxies. In addition, the single, photographic-film sized chip from such amateur CCD cameras coupled with short focal ratio small telescopes can probe extensive sky areas with unprecedented depth, reaching surface brightness levels that are ∼2–3 mag deeper ($\mu_{r,\rm lim} \sim 28$ mag arcsec^{-2}) than both the classic photographic plate surveys (e.g., the Palomar Observatory Sky Survey) and the available large-scale digital surveys (e.g., the SDSS). This offers an alternative and low cost approach for the discovery of low surface brightness galaxies, which may lurk in those regions where the detection efficiency of the available large-scale imaging surveys drops to very small values.

Recently, van Dokkum et al. (2015a) identified 47 low-surface-brightness galaxies in the direction of the Coma cluster using the Dragonfly Telephoto Array. Although they have only obtained a direct distance for one of these galaxies (van Dokkum et al. 2015b), their spatial distribution suggests that they are associated with the Coma cluster. Some of these Coma galaxies have a similar size as the Milky Way (which has an effective radius of 3.6 kpc; Bovy & Rix 2013), but they are significantly redder and more diffuse. They are also fainter than typical low-surface-brightness galaxies (∼24.7 mag arcsec^{-2}; Bothun et al. 1997), and much larger than Local Group dwarf

galaxies (e.g., the effective radius of And XIX, the most extended of the Local Group early-type satellites, is 1.6 kpc; McConnachie et al. 2008). These authors dubbed these galaxies UDGs and defined their key properties to include effective radii greater than 1.5 kpc and central g-band (V-band) surface brightness fainter than 24 (23.6) mag arcsec^{-2}. Although rare, there have been some detections of similar objects in the past. Caldwell et al. (2006) studied two galaxies with similar properties based on their initial discovery by Impey et al. (1988). Based on the tip of the red giant branch (TRGB) distances, these two galaxies are in the core of the Virgo cluster. Both have an effective radius of ~1.5 kpc and a central V-band surface brightness of ~26.5 mag arcsec^{-2}. More recent deep imaging surveys of the Virgo cluster (Ferrarese et al. 2012; Mihos et al. 2015) and the Fornax cluster (Muñoz et al. 2015) have also revealed the presence of faint systems with properties analogous to the UDGs, suggesting that they could belong to a new morphological class of galaxy with the sizes of the giants but the luminosities of the dwarfs.

The origin of these UDGs is not clear. Whether they are only found in clusters or whether they also exist in isolation is still an open question that—when answered—will provide important clues about their formation. van Dokkum et al. (2015a) noted that the spatial distribution of their 47 UDGs avoided the central regions of the Coma cluster, although this apparent location may be an observational selection effect. The large physical sizes of UDG galaxies compared their low stellar masses suggest that they must be dark matter dominated to survive within dense cluster environments. If large numbers of UDGs are found in a range of environments, they may contribute meaningfully to the "missing satellite" problem (e.g., Moore et al. 1999).

During the commissioning of our new project to search for faint satellites around the Local Group spiral galaxies and other nearby systems with amateur telescopes (the DGSAT[19] survey; see Javanmardi et al. 2015), we found an apparently isolated, faint galaxy within the projected extent of the M31 stellar halo, which had been missed by previous surveys that relied on either resolved star counts or the HI 21 cm-radio line for galaxy detection. Although it was initially interpreted as an interesting case of an isolated dwarf spheroidal galaxy, our follow-up spectroscopic observations confirm that this galaxy is at a distance similar to that of the Pisces-Perseus supercluster of galaxies that is in the background of this field of the M31 stellar halo. The properties that we obtain for this background system are very similar to those of the UDGs recently reported by the Dragonfly team (van Dokkum et al. 2015a).

In Section 2 of this paper we describe the discovery of the galaxy and our observing strategy. In Section 3 we detail the photometric and spectroscopic properties that we measure for this galaxy. In Section 4 we discuss the possible nature of DGSAT I as an ultra-diffuse galaxy and speculate about its possible origin.

2. OBSERVATIONS AND DATA REDUCTION

DGSAT I was found in a visual inspection of a full color image of the Andromeda II dwarf galaxy available on the internet and taken by the amateur astronomer Alessandro Maggi using a Takahashi Epsilon 180ED astrograph (18 cmdiameter at $f/2.8$). The detection was confirmed by follow-up observations using the amateur and professional facilities described below. The position of the center of this new dwarf galaxy lies at $\alpha_0 = 01^h\,17^m\,35\overset{s}{.}59$ and $\delta_0 = +33°\,31'\,42\overset{''}{.}37$ (J2000).

2.1. Amateur Telescope Data sets

The first data set was collected with a 15 cm aperture $f/7.3$ Takahashi TOA-150 refractor telescope located at the Fosca Nit Observatory (FNO) at the Montsec Astronomical Park (Ager, Spain). We used a STL−11000 M CCD camera with a large FOV ($1\overset{°}{.}9 \times 1\overset{°}{.}3$, $1\overset{''}{.}69$ pixel^{-1}). A set of individual 1200 s (luminance-filter) images were obtained in photometric nights between 2012 August and September, with a total integration of 43,800 s. Each sub-exposure was reduced following standard procedures for dark subtraction, bias correction, and flat fielding.

Deeper imaging of the field was acquired with a 0.4 m aperture, $f/3.75$ corrected Newton telescope located at the Remote Observatory Southern Alps (ROSA, Verclause, France) in 2013 August. We used a FLI ML16803 CCD detector, which provides a total field of $81' \times 81'$ with a scale of $1\overset{''}{.}237$ pixel^{-1}. The total exposure time in the luminance filter was 13,200 s and the images were reduced using the same standard procedure.

Both images obtained to confirm the discovery of DGSAT I are shown in Figure 1. The luminance images taken with these amateur telescopes were first astrometrically calibrated (Lang et al. 2010), and then calibrated to the SDSS-DR7 (Abazajian et al. 2009) photometric system. To begin the flux calibration of both images, we remove any residual large-scale sky gradients in our wide-field images by modeling the background using a two-dimensional, fourth-order Legendre polynomial that was fitted to the median flux in coarse pixel bins after masking all sources that were detected above the background at $\gtrsim 5\sigma$ level. The bins were typically $5'$ on a side.

We then located 67 isolated stars distributed throughout each image with SDSS r-band magnitude $16 < r < 19$, and performed aperture photometry on them. The same set of stars was measured in both images. The positions of these stars were matched with the SDSS DR7 catalog, from which we retrieved their g, r and i magnitudes. From these data, a linear relation between the r magnitude and the luminance instrumental magnitude was derived individually for each image. We find that the residuals from this relation are a strong linear function of $g - i$ color and vary by 0.5 mag over the color range $0.4 < g-i < 2.7$. Once this color term was corrected, the statistical uncertainty in the flux calibration is only 0.04 mag. The 5σ limiting surface brightness for background variations measured following the procedure of Cooper et al. (2011; see their Appendix) is 27.16 mag arcsec^{-2} and 26.03 mag arcsec^{-2} for the TOA-150 and 0.4 m $f/3$ data, respectively, as determined by measuring the standard deviation of the median of random $20''$ apertures placed around each image. This means that the TOA-150 imaging is ~1 mag deeper than the ROSA 0.4 m data in terms of photon statistics, and its sensitivity to large-scale surface brightness variations is less hindered due to the better quality of the flatfielding.

2.2. Subaru Optical Archive Data

We use a deep image of the field around the And II dSph obtained with the Subaru/SuprimeCam wide field imager

[19] Dwarf Galaxy Survey with Amateur Telescopes.

Figure 1. Follow-up small telescope images of DGSAT I: (top) color image obtained with the FNO TOA-150 refractor; (bottom) luminance filter image obtained with the ROSA 0.4 m telescope. The new dwarf is detected as a small cloud (top left) close to the And II dSph (bottom right), visible only ∼15′ to the west. North is top, east is left. The field of view of these cropped images is ∼19′ × 11′.

(34′ × 27′ FOV, 0.″202 pixel; Miyazaki et al. 2002), which is publicly available from the SMOKA archive (Baba et al. 2002). These observations include dithered exposures of 5 × 440 s in the Subaru *V*-band and 20 × 240 s in the Subaru *I*-band with a seeing around 0.″6 (McConnachie et al. 2007; Ho et al. 2012).

Preprocessing of the data was done by debiasing, trimming, flat fielding, and gain correcting each individual exposure chip-by-chip using median stacks of nightly sky flats. The presence of scattered light due to bright stars both in and out of the field of view required removing this smoothly varying component before performing photometry and solving for a World Coordinate System solution. To remove scattered light, we fitted the smoothly varying component by creating a flat for every chip within each frame by performing a running median with a box size of 300 pixels. This was then subtracted from the original, unsmoothed frame to -produce a final image for photometric processing. The resulting Subaru *V*-band image is given in Figure 2.

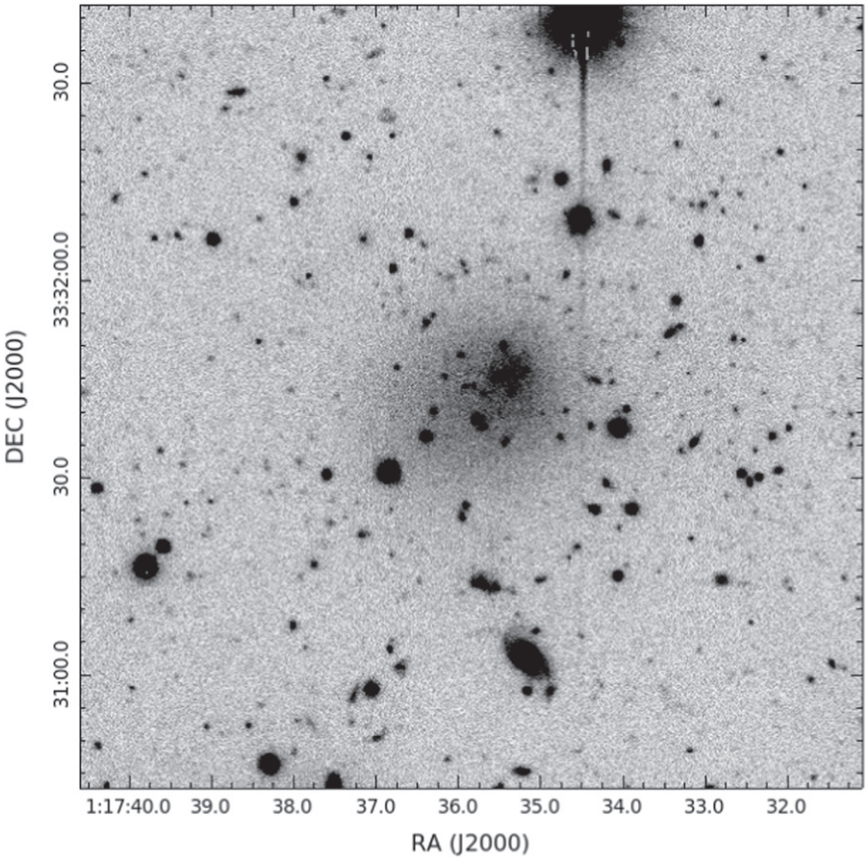

Figure 2. Subaru/SuprimeCam *V*-band image of DGSAT I from the SMOKA archive (see Section 2.2).

Photometric calibration was performed using the DAOPHOT II and ALLSTAR (Stetson 1987) packages. Sources were detected in the *V*-band image by requiring a 3σ-excess above the local background, with the list of detections being subsequently used for the ALLSTAR run on the *I*-band image. To obtain clean CMDs and minimize the contamination by faint background galaxies, sources with the ratio estimator of the pixel-to-pixel scatter $\chi < 2.0$ and sharpness parameters $|S| < 1.0$ (see Stetson 1987) were kept for further analysis. Instrumental magnitudes were obtained by cross-correlating with stellar photometry in the Subaru filter system from McConnachie et al. (2007), kindly provided in digital form, with zero-points determined as resistant mean of the differences between our instrumental and the calibrated Subaru magnitudes (denoted here as V', I'). The accuracy (standard error) of the zero-point is better than 0.03 mag. For the transformation to the standard system we combined Equation (1) in McConnachie et al. (2007), which link the Subaru and the INT filter systems, with the transformation equations for the INT and Johnson/Kron-Cousins systems, available on the INT Wide Field Survey (WFS) webpage.[20] The resulting transformations relations are:

$$V = V' + 0.040 \times (V' - I')$$
$$I = I' - 0.090 \times (V' - I'),$$

where (V, I) and (V', I') are the magnitudes in the standard and Subaru systems, respectively.

2.3. Spectroscopic Observations

During the refereeing process of this paper, spectroscopic observations of DGSAT I were obtained using the primary focus of the 6 m Bolshoi Teleskop Alt-azimutalnyi (BTA) telescope of the Special Astrophysical Observatory of the Russian Academy of Sciences (SAO RAS) with the SCORPIO spectrograph[21] (Afanasiev & Moiseev 2005) on 2014 October 28th–29th. The slit width was $1''$ and its length was $6'$. The instrumental setup included the CCD detector EEV 42–40 with a pixel scale of 0.18 arcmin pixel^{-1} and the grism VPHG1200B (1200 lines mm^{-1}) with a resolution of FWHM $\sim$ 5 Å, a reciprocal dispersion of $\sim$0.9 Å pixel^{-1} and a spectral range of 3700–5500 Å. Two spectra of 12,000 and 13,200 s exposure time were obtained in two consecutive nights under very good atmospheric conditions. At the beginning and at the end of each night a sequence of 10–20 bias frames was recorded. The fluctuations of the bias level were small ($\sim 4\, e^-$). Flatfield and He–Ne–Ar arc calibrations were taken each science exposure, which allowed us to provide a reliable wavelength calibration and a pixel-by-pixel sensitivity correction for our spectra.

The data reduction was performed using the European Southern Observatory Munich Image Data Analysis System (MIDAS; Banse et al. 1983) and the Image Reduction and Analysis Facility (IRAF) software system (Tody 1993). It included bias and dark subtraction, flat-field correction, wavelength calibration, background subtraction and extraction of one-dimensional spectra. The dispersion solution provided an accuracy of the wavelength calibration of $\sim$0.16 Å. Because

[20] http://www.ast.cam.ac.uk/~wfcsur/technical/photom/colours

[21] http://www.sao.ru/hq/lon/SCORPIO/scorpio.html

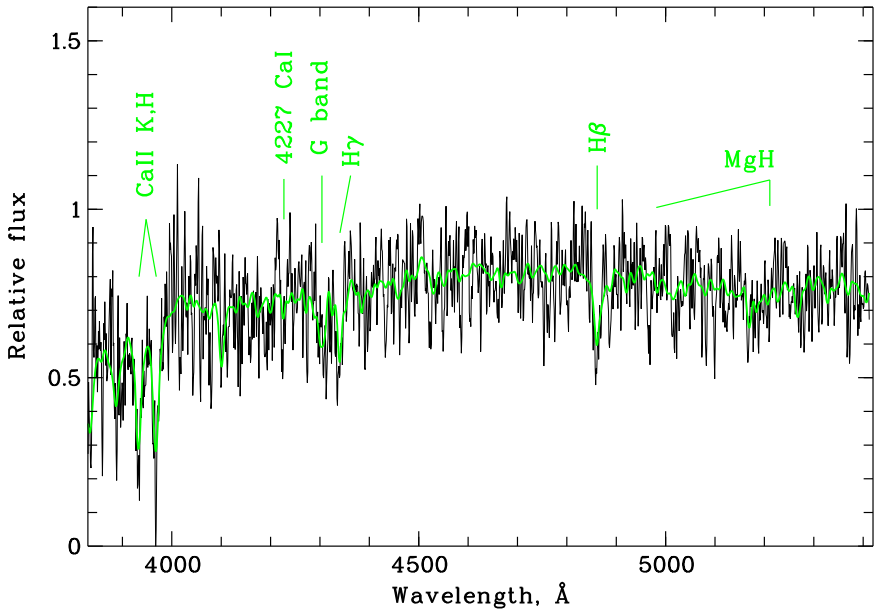

Figure 3. The integrated spectrum of the stellar light of DGSAT I (black) in comparison with a model one (green). The fitting uses the Vazdekis et al. (2010) SSP model composed of intermediate-age metal-rich (age = 1.7 ± 0.4 Gyr, [Fe/H] = −0.2 ± 0.3 dex) population and the MILES stellar library.

our object is of very low surface brightness, accurate subtraction of night sky lines is critical for the correct determination of its radial velocity. The sky background subtraction and correction of the spectrum curvature were done using the *background* task in IRAF. Finally, one-dimensional spectra were extracted from the two-dimensional ones and summed. The signal-to-noise ratio (S/N) in the integrated light spectrum of DGSAT I is ∼5 per wavelength bin and per spatial resolution element. The resulting integrated spectrum is displayed in Figure 3.

2.4. SAO Narrow-band Observations

Narrow-band observations were made with the 6 m telescope at the SAO RAS using the SCORPIO detector with a 2048 × 2048 pixel matrix in a 2 × 2 binning mode and an image scale of 0.″18 pixel^{-1}, which yields a full field of view of 6.′1 × 6.′1. Images in Hα+[NII] and in the continuum were obtained on 2013 October 26, by observing the galaxies through a narrow band Hα filter (FWHM = 75 Å) with an effective wavelength of 6555 Å, and the SED607 (with FWHM = 167 Å, $\lambda = 6063$ Å) and SED707 (with FWHM = 207 Å, $\lambda = 7036$ Å) intermediate band filters for the continuum. The exposure times were 6 × 300 s in the continuum and 3 × 600 s in Hα.

A standard procedure for analysis of direct CCD images was used for processing the data. The bias was initially subtracted from all the data, and then all the images were divided by a flat field. Afterwards, the cosmic ray events were removed and the sky background was measured and subtracted from each image. The continuum images for each pointing were normalized to the corresponding Hα images using 15 field stars so that continuum could be subtracted from the Hα images. The Hα flux was then measured from the continuum subtracted images and calibrated using spectrophotometric exposures of standard stars obtained on the same night. For DGSAT I we detected no Hα emission, with an upper limit for its Hα flux of $\log F(\mathrm{H}\alpha)$ (ergs^{-1} cm^{-2}) < -15.8. This limit will be used to set constraints on the stellar populations in Section 3.4.

3. RESULTS

3.1. Color–Magnitude Diagrams

Figure 4 shows the CMD of a selected region of 8.′15 × 15.′03 from the Subaru field (corrected for Galactic extinction $A_B = 0.27$) with RGB stars from the halo of M31 and some Galactic foreground stars at $(V - I)_0 \geqslant 2.0$. Based on the densely populated CMDs from the PAndAS survey (McConnachie et al. 2009) of M31's halo (e.g., Figure 4 in Conn et al. 2011), we selected stars with $(V - I)_0 \leqslant 2.0$ for our sample, eliminating most of the Galactic foreground population but still keeping most of the stars in M31's halo and potential resolved stellar sources in the dwarf galaxy. Using a similar color criterion as Conn et al. (2012) to select putative RGB stars in the satellite candidate (Figure 4), we find that only 17 stars fall in this area of the CMD and within 40″ of the center of the galaxy, consistent with the average density of stars within these color cuts in the image. Hence, no significant over-density of resolved RGB stars is found at the location of DGSAT I that would indicate it is a dwarf satellite of M31. This is consistent with the lack of detection of this object in the list of over-density candidates in this region of Andromeda from the PAndAs survey (Martin et al. 2013). Thus, we conclude that the galaxy is not resolved into stars. This further rejects the possibility that DGSAT I is a companion of the more distant spiral galaxy NGC 404 that is 2.°75 distant in projection (∼3.13 Mpc; Williams et al. 2010). It is also very unlikely that it is a dwarf member of any other galaxy group in the background of M31 in the local universe (e.g., NGC 672 with five known companions or NGC 891 with 18 known companions).

3.2. Radial Velocity and Distance

To derive radial velocities of our object we used: (a) the *fxcor* task in IRAF; and (b) the ULySS program (Koleva et al. 2008, 2009) with Vazdekis et al.'s (2010) SSP model, the Salpeter IMF (Salpeter 1955) and the MILES stellar library (Sanchez-Blazquez et al. 2006). The task *fxcor* uses the Fourier

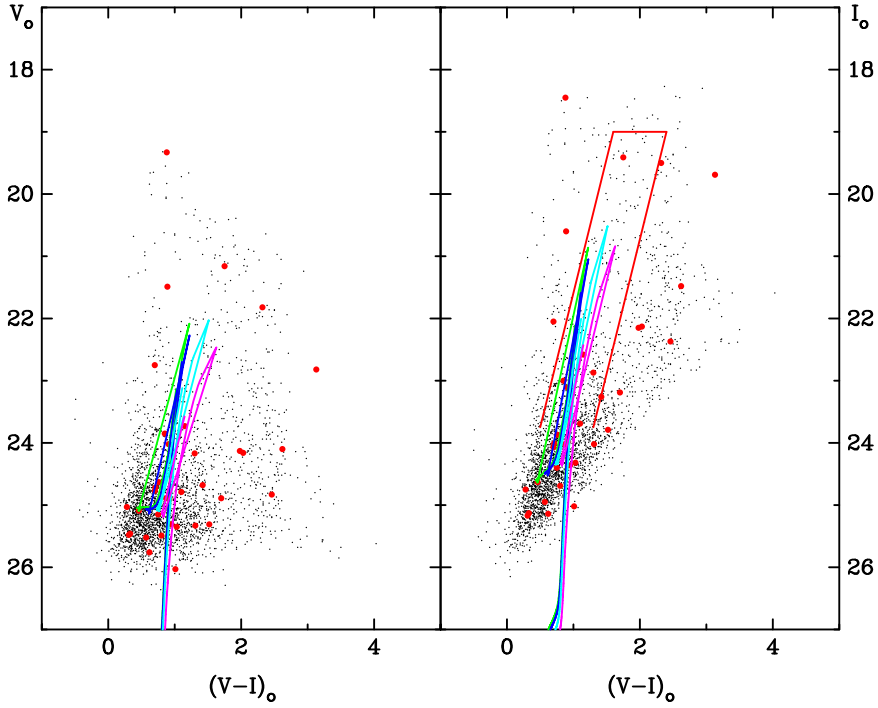

Figure 4. Dereddened color–magnitude diagrams of resolved stars in the Subaru/SuprimeCam field (black dots) and within 40″ (red circles) with sharpness $|S| \leqslant 1$ and $\chi < 2.0$ parameters. The isochrones (Chen et al. 2014) for populations at a distance modulus for the Andromeda galaxy of 24.6, age 9.8 Gyr, $[\alpha/\mathrm{Fe}] = +0.2$ and metallicities $Z = 1.5 \times 10^{-4}$ (green), 2.4×10^{-4} (dark blue), 6.0×10^{-4} (pale blue) and 1.4×10^{-3} (pink) are indicated, along with the selection box (red) for resolved RGB stars, which is very similar to the one used for the detection of the TRGB in fields around M31 (Conn et al. 2012).

cross-correlation method developed by Tonry & Davis (1979). The resulting radial velocity is $V_h = 5453 \pm 111\,\mathrm{km\,s^{-1}}$. The cross-correlation peak is weak and the velocity error is large because of the low S/N in the spectrum.

The ULySS program provides more accurate results than *fxcor*, because it allows one to take into account the line-spread function (LSF) of the spectrograph, viz. the variation of the measured velocity and instrumental velocity dispersion as a function of wavelength (Koleva et al. 2008). The LSF was approximated by comparing a model spectrum of the Sun to twilight spectra taken during the same night as the studied object. The result is $V_h = 5450 \pm 40\,\mathrm{km\,s^{-1}}$. Using the prescriptions of Tully et al. (2008), we transform our initial measured velocity to one relative to the motion of the Local Group and obtain $V_{\mathrm{LG}} = 5718 \pm 40\,\mathrm{km\,s^{-1}}$. This radial velocity corresponds to the Hubble distance of 78 ± 1 Mpc for $H_0 = 73\,\mathrm{km\,s^{-1}\,Mpc^{-1}}$. The estimated velocity dispersion in the galaxy is $\sigma_V \sim 100\,\mathrm{km\,s^{-1}}$. The σ_V value is very approximate given the low S/N in the spectrum of DGSAT I and needs to be verified at higher resolution and at higher S/N.

Interestingly, this velocity is consistent with those of the Pisces-Perseus supercluster, which has typical velocities in the range of 4800–5400 $\mathrm{km\,s^{-1}}$. Figure 5 shows the position of DGSAT I, clearly overlapping a prominent filament of this supercluster in this sky region (Wegner et al. 1993) and in proximity to some of the massive members of this structure (NGC 383 and NGC 507, at projected distances of 2–3 Mpc). Therefore DGSAT I could well be part of this structure, lending support to our redshift distance estimate, with a corresponding diameter (effective size) near ∼10 kpc (see the next section). Its simultaneous low surface brightness (∼25 mag $\mathrm{arcsec^{-2}}$) and large physical extent would place it in the category of the *ultra-diffuse* galaxies (see Section 4).

3.3. Structural Properties and Surface Brightness Profile

The structural parameters of the dwarf galaxy were determined by running GALFIT3 (Peng et al. 2010) on the sky-subtracted Subaru *V*- and *I*-band images, with foreground and background objects removed. We characterize the photometric properties of the galaxy by using GALFIT3 to fit a two-dimensional Sérsic profile,

$$I(R) = I_c \exp\left[-b_n (R/R_e)^{1/n}\right]$$
$$I_c \;=\; I(0) = F_{\mathrm{tot}}\,[2\pi q n (R_e b_n^{-n})^2 \Gamma(2n)]^{-1},$$

where I is the surface brightness within ellipses with semimajor axes R, and Γ is the Gamma function. The conversion to the magnitude system (see Table 1) is given by $\mu(R) = \mathrm{ZP} - 2.5\log I(R)$, where ZP is the magnitude zero-point and $\mu_c = \mu(0)$ the central surface brightness. The total flux F_{tot} (expressed as magnitude, $m = \mathrm{ZP} - 2.5\log F_{\mathrm{tot}}$), the effective radius R_e, Sérsic index n, and axis ratio $q = b/a$ are adjustable parameters. The constant b_n is determined by the requirement $F(<R_e) \propto \int_0^{R_e} I(R) R\,dR = F_{\mathrm{tot}}/2$. The geometry of the light distribution is additionally characterized by the location of the profile center and the position angle of the semimajor axis.

We perform masking of intervening objects (mostly foreground stars) and background subtraction iteratively with SExtractor (Bertin & Arnouts 1996) in the area where we fit our model (280″ × 280″), and add user-defined masked regions around the brightest stars. In order to obtain the background reliably, we also mask the target galaxy generously "by hand." After a first pass of simultaneous object detection and background estimation, the task is repeated with the previously detected objects masked, which gives us a more accurate local

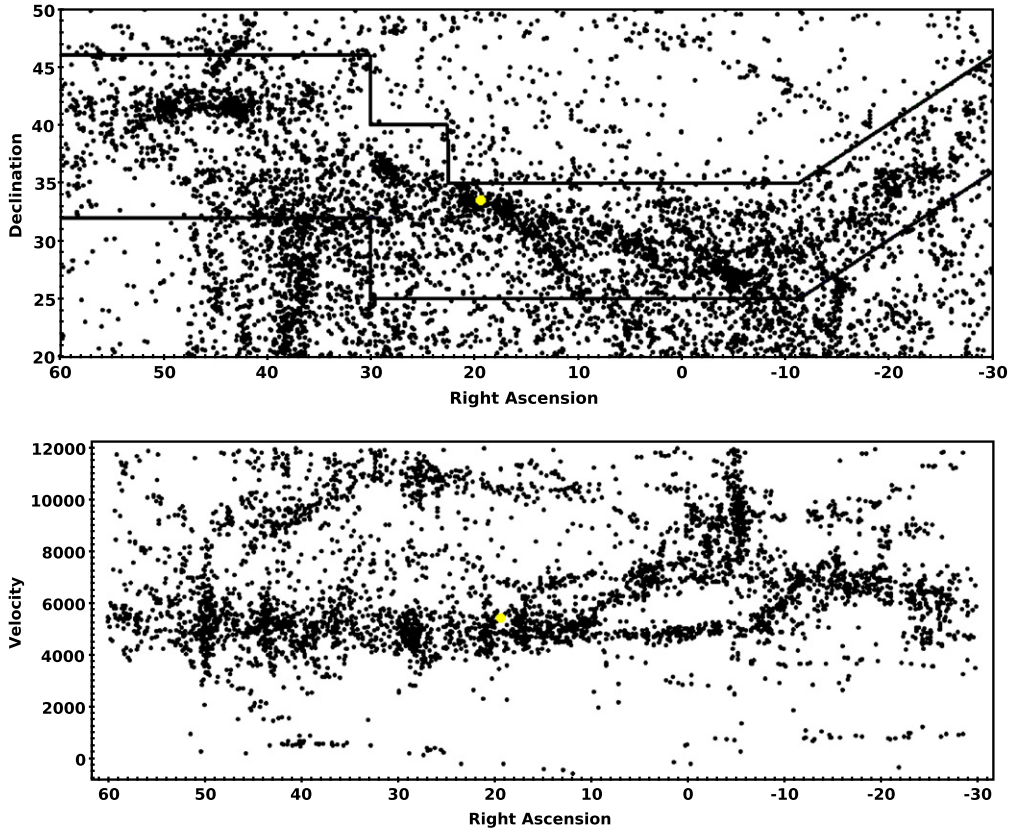

Figure 5. Position and measured radial velocity of DGSAT I overplotted on the available redshift data for the Pisces-Perseus supercluster, following Wegner et al. (1993). The redshift data set includes measurements from the ALFALFA survey and preliminary ones from the on-going Arecibo Pisces-Perseus Supercluster survey (APPSS). Courtesy of M.P. Haynes and the ALFALFA/APPSS team.

Table 1
GALFIT3 Model Photometric Properties of DGSAT I in Our Subaru Images, Calibrated to the Johnson *V*- and *I*-Bands

	Band	Alternative Models		Adopted Model	Modeling Uncertainty
		Model 1	Model 2	Model 3	
Treatment of blue Central over-density		fitted as part of the galaxy	separately modeled by an additional component	masked before fitting	
	V	18.13	18.19	18.18	0.03
m (mag)	*I*	17.15	17.23	17.17	0.04
	V − *I*	0.99	0.97	1.01	0.02
	V	24.46	24.93	24.76	0.24
μ_c (mag arcsec^{-2})	*I*	23.82	24.21	23.97	0.20
	V − *I*	0.65	0.72	0.81	0.08
	V	11.3	12.2	11.7	0.5
R_e (arcsec)	*I*	12.1	13.1	12.5	0.5
	V	0.80	0.62	0.68	0.09
n	*I*	0.69	0.58	0.63	0.06
	V	0.89	0.87	0.88	0.01
b/*a*	*I*	0.87	0.87	0.87	0.01

Note. Rows list (from top to bottom and separately for each band) the extinction-corrected apparent magnitude and color, central surface brightness and central color, effective radius, Sérsic index, and axis ratio of the 2D-SÉrsic profile. In addition to the adopted model ("Model 3", last column), we show results for two alternative models that differ from the adopted model in the way the central blue over-density is treated. Model 1 was fit with a single Sérsic and the overdense region left unmasked. Model 2 accounts for this feature by adding a second Sérsic component. Model 3, which is our preferred model (see also Figure 6), was fitted after masking the over-density, but is otherwise the same as the alternative Model 1: a single Sérsic component with a 1st-order fourier mode to allow for the lopsidedness. The final column gives the standard deviation between the models as an estimate of the systematic uncertainty, i.e., uncertainty in the choice of model used to parametrize of the light distribution.

background level and background noise, and thus also a more complete object mask. Finally, by reapplying SExtractor on the GALFIT residual image, we eventually also mask previously undetected objects that overlap with our target.

The noise map, which enters the χ^2 computation during fitting, was constructed by measuring the noise in the background and adding in quadrature the Poisson noise of the sources. In lieu of including the sky background as a free

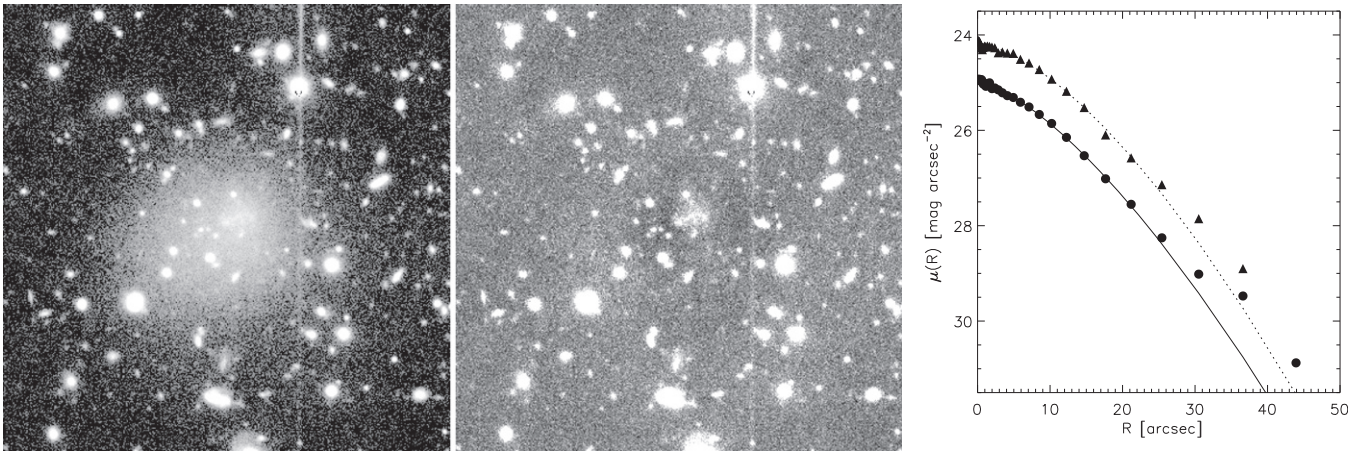

Figure 6. GALFIT analysis and surface brightness profile of DGSAT I. Left panel: cutout from the *I*-band image, 80″ on a side (north up, east left). Middle panel: best-fit residuals (data minus model) of our adopted GALFIT model (Model 3, see Section 3.3 and Table 1). The data image is displayed on a logarithmic grayscale ranging from 28.5 (black) to 23.5 mag arcsec^{-2} (white); a linear scale and a range of ±25 mag arcsec^{-2} was used for the residual image. Note the lopsidedness of the galaxy, as well as the conspicuous near-central over-density, which is irregularly shaped and flocculent, yet elongated (roughly along the east–west direction), and was masked during the fit. The *V*-band images are very similar and not shown here. Right panel: surface brightness profile $\mu(R)$ along the semimajor axis of data and model, displayed respectively as circles and solid line (*V*-band), as well as triangles and dotted line (*I*-band). The model agrees with the data well except at $R \gtrsim 25''$ ($\approx 2R_e$), where it underestimates the surface brightness by ≈0.5 mag.

parameter in the GALFIT model, which can induce degeneracy in the output model parameters, we subtract the background from the image before fitting. Lastly, to account for the effect of seeing and telescope optics, we construct a model image of the PSF using several bright, unsaturated foreground stars near the position of DGSAT I in the image. This empirically derived PSF model is convolved with the GALFIT model before comparison to the image data.

We first fit a 2D-Sérsic profile as a basic model of the *V*- and *I*-light distribution of DGSAT IIn this simple model, we find DGSAT I is almost circular ($b/a \sim 0.9$) with a shallow, sub-exponential inner profile ($n < 1$), both of which are typical structural characteristics for galaxies of dwarf spheroidal morphology. However, despite the overall agreement of the model with the data (see Figure 6), the data show two peculiarities with respect to the smooth regular Sérsic model.

First, there is a faint, fuzzy irregularly shaped elongated over-density of ∼6″ length near, but not coinciding with, the galaxy center (offset by ∼1″). Apart from its shape, the over-density also differs from the main body of the galaxy by its bluer color, more specifically $V - I = 0.7$ for the over-density as compared to $V - I = 1.0$ for a regions at a similar radius within DGSAT IIDue to its small angular size and the spatial resolution of our ground-based imaging, it is not possible to shed additional light on the nature of the blue over-density at this time (see also Section 3.4). It could be an unresolved clump of young stars overlapping the smooth (and possibly older) component of the galaxy, similar to those observed in some nearby dIrr galaxies (e.g., Sextans A, that contains a conspicuous, off-center star formation region; Dohm-Palmer et al. 1997). Alternatively, DGSAT I could be a nucleated UDGs, similar to those found in the Virgo cluster (Beasley et al. 2016; Mihos et al. 2015).

For this reason, we construct three GALFIT3 models that differ in how this blue off-center over-density is treated. Model 1 assumes that it should be included in the fit, and leaves it unmasked. Model 2 also leaves it unmasked, but accounts for it as an additional structural component with fully independent parameters from the main body of the galaxy (i.e., both the general parameters and those specific to the Sérsicf˛it). In Model 3 we exclude the over-density from the fit by masking it. Table 1 compares the resulting parameters of the main component (the sole component in Model 1 and Model 3). Parameters generally vary only mildly between these models, by ∼0.01 for m, R_e and $q = b/a$. Differences in the best-fit μ_c and n are more pronounced (∼0.1) as they more specifically reflect the central profile.

Another peculiarity in the light distribution of DGSAT is its significant lopsidedness: the center of the innermost isophotes are offset from those of the outermost isophotes by several arcseconds to the north–west. We accommodate for the apparent lopsidedness by allowing a first-order Fourier mode in the model isophotes. The best-fit amplitude of the mode is 0.21 (0.15) in *V*-band (*I*-band). Although allowing for the Fourier mode in a single-component system is not essential to obtain accurate flux and scale parameters, this modification to the model is useful for us since it provides a measurement of the galaxy center and a realistic set of isophotes, which we utilize to measure the surface brightness profile $\mu(R)$ with the IRAF task *ellipse* (see below).

When measuring $\mu(R)$ on the data image, we use the isophotes of the model. Fitting the isophote geometry simultaneously with $\mu(R)$ (which was done on the model image) is impeded at small radii due to the low central surface brightness, the extremely shallow central gradient, and the irregularities introduced by the off-center over-density and remaining small contaminants.

For the following discussion of the DGSAT I properties, we select Model 3 (where the over-density is masked) as our adopted model. We do not base this selection on the value of χ^2 at the best-fit parameters, since it is very similar for all three models considered.[22] We assume that, given its different color and presumably younger population, this over-density is a peculiar feature of DGSAT I and its light is not reflective of the global properties (including the stellar mass) at same confidence as as in the smooth, red component of the galaxy.

[22] Regardless, the minimum-χ^2 of different models generally does not provide statistically well-defined quantitative evidence for intercomparison of models.

Table 2
Summary of DGSAT I Properties, Assuming our Redshift Distance of 78 Mpc

Quantity	Notation	Value
Right Ascension	R.A.	$01^h\ 17^m\ 35\overset{s}{.}59$
Declination	decl.	$+\ 33°31'42\overset{''}{.}37$
Radial velocity (heliocentric)	V_h	(5450 ± 40) km s^{-1}
Hubble distance	D	(78 ± 1) Mpc
Apparent magnitude	m_V	18.18 ± 0.04
	m_I	17.17 ± 0.05
Central surface brightness	$\mu_{c,V}$	(24.8 ± 0.2) mag arcsec^{-2}
	$\mu_{c,I}$	(24.0 ± 0.2) mag arcsec^{-2}
Absolute magnitude	M_V	-16.3 ± 0.1
	M_I	-17.3 ± 0.1
Luminosity	L_V	$(2.7 \pm 0.2) \times 10^8\ L_{\odot,V}$
	L_I	$(3.6 \pm 0.2) \times 10^8\ L_{\odot,I}$
Total color	$V - I$	1.0 ± 0.1
Central color	$(V - I)_c$	0.8 ± 0.1 (0.71 ± 0.02)
Effective radius	$R_{e,\ I}$	(4.7 ± 0.2) kpc
Axis ratio	$q_I = (b/a)_I$	0.87 ± 0.01
Sérsic index	n_I	0.6 ± 0.1
Over-density luminosity		$\sim 7 \times 10^6\ L_{\odot,V}$ (~2.5% of DGSAT I)
		$\sim 4 \times 10^6\ L_{\odot,I}$ (~1.1% of DGSAT I)
Over-density effective radius		~1.0 kpc (both bands, ~22% of DGSAT I)
Stellar mass-to-light ratio in I-band	$M_\star/L_I$	$1.1\ M_\odot/L_{\odot,I}$
Stellar mass	$M_\star$	$4.0 \times 10^8\ M_\odot$
Gas mass (HI)	$\log M_{\rm HI}(M_\odot)$	<8.8
Hαflux	$\log F(\mathrm{H}\alpha)$ (ergs^{-1} cm^{-2})	<-15.8
Star formation rate	$\log$ SFR ($M_\odot$ yr^{-1})	<-2.6
Specific star formation rate	$\log$ sSFR (yr^{-1})	<-11

Note. The extinction-corrected apparent magnitudes in the standard (Johnson-Cousins) V- and I-band, central surface brightness, luminosity, axis ratio and size are the best-fit GALFIT3 2D-Sérsic profile constrained by our subaru images (see Section 3.3). R_e, b/a and n are given for the I-band, but differ from V only at the percent level. For the central color, two values are given: the central magnitude difference of the Sérsic models in the two bands, and (in brackets) as measured in a small $1\overset{''}{.}4 \times 0\overset{''}{.}6$ elliptical aperture. The photometric errors give the approximate systematic uncertainty from the choice of parametric model, except for the aperture-based central color where it is based on a Monte-Carlo realization of the aperture geometry. The error in distance and the calibration error of 0.03 mag was added in quadrature where applicable, while random errors from pixel noise are negligible and ignored. Due to the unknown systematic uncertainty in $M_\star/L_I$, no errors are given here and for the derived $M_\star$.

A *rough* estimate of the flux and size of this over-density can be obtained from the extra-component fitted in Model 2, yielding 2.5% flux fraction in the V-band (1.1% in the I-band), and 22% of the effective radius (both bands; see Table 2).

The apparent galaxy parameters (Table 1, column for "Model 3") translate to physical parameters using our adopted redshift distance of 78 Mpc. The extinction-corrected apparent I-band magnitude of 17.17 implies an absolute magnitude, $M_I = -17.29$, and, adopting $M_{\odot,I} = 4.1$ (Binney & Merrifield 1998), a luminosity $L_I = 3.6 \times 10^8 L_{\odot,I}$. In the V-band, we obtain $m_V = 18.18$, which implies an absolute magnitude, $M_V = -16.28$ and, with $M_{\odot,V} = 4.8$, $L_V = 2.7 \times 10^8\ L_{\odot,V}$. At the same time, the effective radius of $12\overset{''}{.}5$ translates to 4.7 kpc. There is some uncertainty in R_e, both due to the variation with band as well as due to background uncertainty; we give here the maximum range of R_e resulting from fitting different models *and* both bands (see above and Table 1), which is $(13\overset{''}{.}1–11\overset{''}{.}3)/2 = 0\overset{''}{.}9$, hence ≈10% or ≈0.5 kpc maximum range in R_e. Thus, this galaxy is very extended (about Milky-Way sized; Bovy & Rix 2013) for its luminosity (which is less than 1/100 of the Milky Way).

3.4. Stellar Mass and Star Formation Rate (SFR)

In order to estimate the stellar mass of DGSAT I we use the work of Zibetti et al. (2010), who provide mass-to-light ratios ($M_\star/L$) in SDSS bands for galaxy stellar populations as a function of one or more colors. They also show that the mass-to-light ratio in the i-band is well determined (low scatter and low dust effects) by one color alone, $g - i$. Fortunately, our Subaru images provide photometry in closely related bands, however we still need to transform the Johnson-Cousins system to the SDSS system.

With only one color at hand, we have little knowledge of the stellar population parameters (primarily age and metallicity) that effect the transformation between photometric bands. We refer to Jordi et al. (2006) when calculating $g - i = 1.481 \times (V - I) - 0.536 = 0.960$ with our measured $V - I = 1.01$; this transformation is based on Stetson's extension of the Landolt standard stars and hence a mix of stellar populations. A transformation from Johnson I to SDSS i is unfortunately not possible from the tables provided in Jordi et al. (2006); we rely on the relations of R. Lupton, which are available on the SDSS website[23] and use the same set of standard stars. We obtain $m_i \equiv i = I + 0.127 \times (V - I) + 0.320 = 17.62$, corresponding to $\log(L_i/L_{\odot,i}) = 8.57$ when adopting an absolute solar magnitude of $M_{\odot,i} = 4.58$ (Blanton et al. 2003). With $\log[(M_\star/L_i)\ /\ (M_\odot/L_{\odot,i})] = 0.963 + 1.032 \times (g - i)$, we obtain a stellar mass-to-light ratio $M_\star/L_i = 1.07\ M_\odot/L_{\odot,i}$ and a stellar mass for DGSAT I of $M_\star = 4.0 \times 10^8 M_\odot$.

We mention that the stellar M/L is an uncertain quantity; among other factors it is sensitive to priors in the star formation history and assumptions on the shape of the stellar initial mass function. For example, the relations of Bell et al. (2003) yield $M_\star/L_i = 2.2\ M_\odot/L_{\odot,i}$ for the same $g - i$ color; a factor of two higher than the result based on Zibetti et al. For comparison, using either only Population-I stars or Population-II stars, $g - i$ is 0.97 or 0.93, i.e., the stellar population effects the color transformation by ~0.04 mag, and thus M/L_i by a factor of $\lesssim$0.04. The i-band magnitude is even less sensitive to stellar population differences than the $g - i$ color. For example, using the SDSS-Johnson transformation derived for Population-I stars from Jordi et al., in conjunction with $R - I$ colors from Caldwell et al. (1993), m_i differs by a mere 0.002 mag from our adopted transformation using all standard stars.

However, the relatively large systematic uncertainty in $M_\star/L$ does not effect the conclusions of our study: that DGSAT I is extremely extended for its mass (or luminosity) and therefore may represent a possible class of peculiar galaxies with an

[23] https://www.sdss3.org/dr8/algorithms/sdssUBVRITransform.php

extremely low surface brightness (that is typical of the much smaller dSph galaxies) for their mass (or size). We therefore attempt to explore further properties of DGSAT-I from the available data, namely Hα flux, SFR, and HI content, that may help to shed light on its formation.

The lack of spatially extended emission lines in the SAO spectra (see Section 2.3) is consistent with our Hα-band observations and rules out the possibility of this object being a nearby star-forming galaxy. This is also consistent with the observed upper limit of Hα flux detected in our SAO narrow band observations (Section 2.4). We also note that DGSAT I was not detected in the 21 cm survey of this filament of the Pisces-Perseus superclusters by Giovanelli & Haynes (1989). Taking the upper limit for the flux of this survey, $F(\mathrm{HI}) = 0.5\,\mathrm{Jy\,km\,s^{-1}}$(with signal-to-noise S/N $\sim$ 5), this yields $\log M_{\mathrm{HI}}(M_\odot) < 8.76$.[24] We hence estimate the logarithm of the ratio of HI-to-total stellar masses, $\log M_{\mathrm{HI}}/M_\star < 0.16$. Accepting this upper limit, implies about as much mass in HI as in stars. This is, for example, four times HI fraction than that found in the LMC (Kim et al. 1998), which has one of the highest HI fractions of the galaxies in the local universe. Therefore we conclude that the upper-limit estimate is a very conservative one, and presume that M_{HI} of DGSAT I is actually at least one magnitude lower.

Following Kennicutt (1998), we determined the integral SFR in DGSAT I by the relation,

$$\log \mathrm{SFR}(M_\odot\ \mathrm{yr}^{-1}) = 8.98 + 2\log(D\,[\mathrm{Mpc}]) + \log(F_c(\mathrm{H}\alpha)) \quad (1)$$

where $F_c(\mathrm{H}\alpha)$ is its integral flux F in the Hα line in erg cm^{-2} s (see Section 2.4), corrected for the Galactic extinction $A(\mathrm{H}\alpha) = 0.538A_B$ (Schlegel et al. 1998, with $A_B = 0.27$). The internal extinction in the dwarf galaxy itself was considered negligible. Therefore, for the distance of DGSAT I, we obtain an upper limit of $\log(\mathrm{SFR}(M_\odot\,\mathrm{yr}^{-1})) < -2.56$. The corresponding upper limit for the specific star formation rate (sSFR; the SFR per unit galaxy stellar mass) is sSFR < -11.16.

Karachentsev & Kaisina (2013) discussed star formation properties of Local Volume galaxies. The SFR of DGSAT I is somewhat low for its upper limit HI mass, but still consistent with the spread in their sample (see their Figure 5). They showed that the median value of the sSFR does not change significantly for local volume galaxies with neutral hydrogen masses in the range $7 < \log M_{\mathrm{HI}}\ (M_\odot) < 9.5$. Most galaxies have $\log \mathrm{sSFR}(\mathrm{yr}^{-1}) \sim -10$, but with a large scatter toward the lower sSFR over the whole range of M_{HI}. Some objects with neutral hydrogen masses in the range $7 < \log M_{\mathrm{HI}}\ [M_\odot] < 9.5$ reach logarithmic sSFRs as low as ~ -15. Thus, the upper-limit sSFR and SFR/M_{HI} ratio of DGSAT I is consistent with their Local Volume study, and comparable with the values typical for quenched galaxies. However, SFR or hydrogen mass may also be much lower, a possibility that will have to await additional data to be tested.

DGSAT I displays a clear off-center over-density discussed in Section 3.3 (clearly visible in Figures 2 and 7). This raises the question of whether this feature harbors a young stellar population, originating in its last episode of star formation. Interestingly, irregardless of the our treatment of the blue over-density in our GALFIT3 modeling (Table 1), the central $V-I$ color of the Sérsic profile is still $\sim$0.2 mag bluer than its global mean color (compare the $V-I$ rows in the top two sections, m and μ_c, in Table 1). It is not clear if this difference is real or an artifact from profile mismatch or background uncertainties. Thus, we perform an additional test by comparing the mean color in two different regions: (1) a circular annulus between $4'' < R < 15''$ from the center of DGSAT I and (2) a small elliptical aperture at the center with semimajor and minor axes $a = 1\farcs4$, $b = 0\farcs6$ with a position angle of PA $= 10°$ north–west. These two annuli are indicated in the left panel of Figure 7(and described in the caption). As can be seen in Figure 7, these two regions are largely selected based on the features of the $V-I$ color map, with the region (1) selected to both average over background fluctuations but also to avoid contamination from the blue over-density and region (2) selected to sample the core of the object. From this analysis, we find for region (1) $V-I = 1.00$ and for region (2) $V-I = 0.71$, which broadly confirms the bluer nature of the center as measured in the GALFIT3 modeling (Table 1). To ascertain the significance of this finding and evaluate any subjectivity in the definition of the regions, we perform a Monte-Carlo re-analysis with $N = 400$ samples, where the (i) center and (ii) specific parameters for the region shapes are allowed to vary. More specifically, for region (1), the inner and outer radius and for region (2), the semimajor and semiminor axes (a, b) as well as the position angle. The center is allowed to shift by 20% of the harmonic axis mean ($0.2\sqrt{ab}$), the direction of the shift is random, R_{in}, R_{out}, a and b are varied by $\pm$20% of their given value, and PA by $\pm 10°$. All variations are independent of one another and uniformly distributed within their bounds. As a result, the geometric color uncertainty is small, with a standard deviation of 0.01(0.02) mag in the outer (central) aperture, which confirms that the bluer color for the center is robust.

It is difficult to assess with the current data what this 0.3 mag color difference in the center implies about a possible stellar population gradient. The color offset, location and shape of the over-density is similar to those reported for dwarf elliptical (dE) galaxies by Lisker et al. (2006), which were interpreted as the presence of young stars overlaying the mass-dominant old population. It is therefore likely that the bluer color of the over-density feature of DGSAT I ($V-I \sim 0.7$) indicates the presence of young stars from a recent episode of star formation in this region of the galaxy.

4. DISCUSSION AND CONCLUSIONS

We report the discovery of DGSAT I a faint galaxy at a projected distance of 15′ from the Andromeda II dwarf satellite. Its appearance, structural properties and absence of emission lines initially suggested an interesting case of an isolated dwarf galaxy well beyond the Local Group, with a surface brightness and structural properties similar to those of the classical MW dSphs like Fornax or Sculptor. However, our measured line of sight radial velocity ($5450 \pm 40\,\mathrm{km\,s^{-1}}$) reveals that DGSAT I is a background system placed at a distance of $\sim$78 Mpc and possibly associated with the filament of the Pisces-Perseus supercluster projected in this direction of the sky (see Figure 5).

With $\mu_{c,V} = 24.8$ mag arcsec^{-2}, $R_e = 4.7$ kpc, $b/a = 0.9$ and $V-I = 1.0$, the central surface brightness, structural properties, and color are consistent with those of the UDGs recently reported in the Coma cluster (Koda et al. 2015; van Dokkum

[24] DGSAT I is also within the ALFALFA survey zone, but the HI data for this decl. are not yet available.

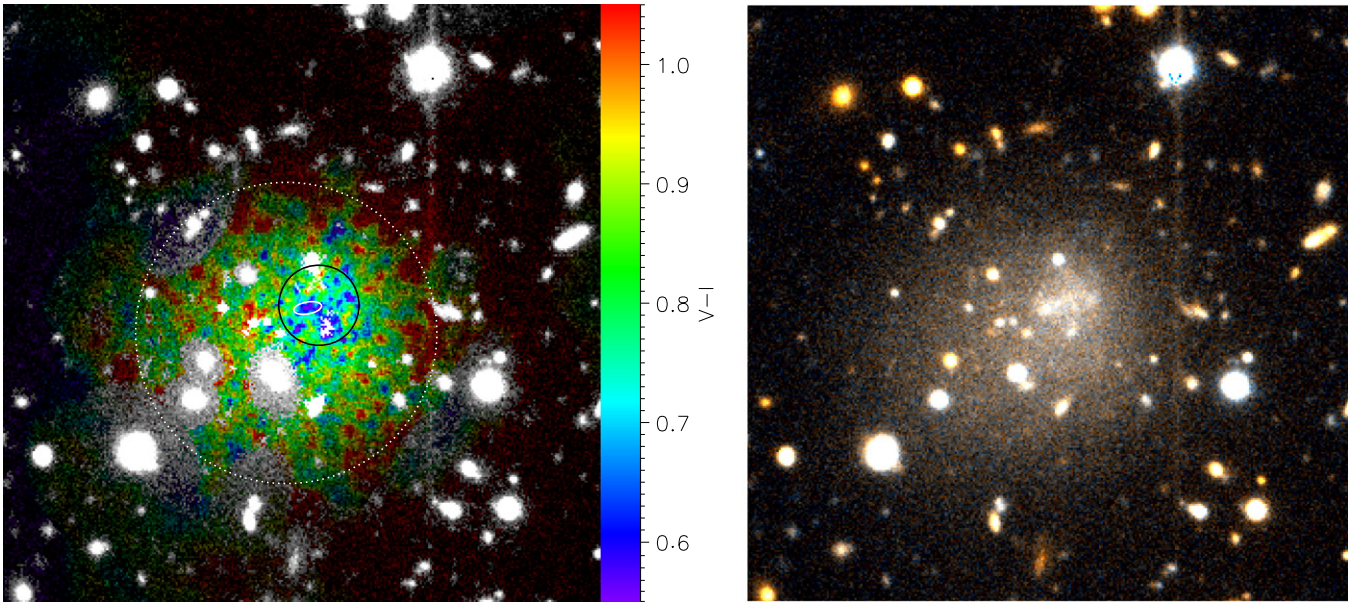

Figure 7. Left panel: the $V - I$ color map of DGSAT I, derived by dividing the Subaru V- and I-band images, after an adaptive boxcar smoothing that ensures a signal-to-noise ratio of S/N > 10 in the flux ratio. Color values are corrected for Galactic foreground extinction, and pixels that were masked for photometry are displayed on a grayscale instead of color. The over-density slightly offset from the galaxy center stands out by its bluer $V - I$ index. Indeed, measuring the color in two apertures, one large circular annulus with $4 < R < 15''$ from the center (the area between the solid black and dotted white circles), and a small elliptical aperture (solid white) with semiaxes $a = 1\farcs4$, $b = 0\farcs6$, we find $V - I = 1.00$ and 0.71 respectively (see Section 3.3). Right panel: a true-color map of DGSAT I, with red and blue channels proportional to I- and V-band flux, and the green channel representing the mean of V and I-band. Although the color contrast is naturally lower here, the center-offset over-density is recognized as mostly white against the orange–gray of the outer part of the galaxy. Both images are $1'$ on a side and intensity scaled linearly with surface brightness.

et al. 2015a). These galaxies have g-band central magnitudes of 24–26 mag arcsec^{-2}, effective radii of 1.5–4.5 kpc and appear nearly round on the sky with typical axis ratios of 0.8, and $g - i \sim 0.8$. van Dokkum et al. (2015a) fitted a a Sérsic index of $n = 1$ to their surface brightness profiles, but noted that the data were fit equally well with indices varying from $n = 0.5$ to $n = 1.5$. In the case of DGSAT I, our Subaru images are deep enough for a robust 2D-profile fit, which yields $n \sim 0.6$. The absence of a clear disk structure or spiral arms in the Subaru deep image of DGSAT I supports van Dokkum's suggestion that these objects do not resemble the classical low-surface brightness galaxies well known in the literature. This is also consistent with the gas content and integral SFR of DGSAT I that we found in Section 3.4, which are typical for quenched galaxies.

Thus, DGSAT I is the first ultra-diffuse galaxy found in the Pisces-Perseus supercluster. However, unlike these previous detected UDGs, DGSAT I is almost a *field* UDGs and is located in a sky region with a significant lower density of massive galaxies than those found in the center of the Coma, Virgo or Fornax galaxy clusters.

The formation mechanism for these ultra diffuse galaxies is unknown. They have only been found in clusters so far (as is also the case for quenched dwarf galaxies; Gavazzi et al. 2010; Geha et al. 2012) and their Sersic indices, sizes, red colors and round morphologies resemble the most extended dEs (e.g., Geha et al. 2003; Toloba et al. 2014). Thus, one possibility is that they are the products of environmental effects affecting a progenitor population that falls into a cluster. The structural properties of these diffuse galaxies suggest that they are the extension to larger sizes of dwarf early-type galaxies (dEs; see Figure 8). DGSAT I also has a mass in the range of those of dEs (e.g., Toloba et al. 2014), and its blue off-center kpc-scale over-density closely resembles those found in dEs as well (Lisker et al. 2006).

Tidal effects (including harassment, stripping, stirring, and heating) are environmental mechanisms produced by gravitational interactions between galaxies (Moore et al. 1998; Mayer et al. 2001; Mastropietro et al. 2005). Stripping and mass loss tend to reduce the sizes of the affected galaxies, making this an unlikely pathway to forming these ultra diffuse galaxies. However, some infalling galaxies could experience milder tidal heating effects. In fact, Gnedin (2003) simulated tidal heating of low-surface-brightness disk galaxies in clusters, and found the disks could be completely transformed into spheroids while losing few of their stars and remaining large in size. In combination with ram pressure stripping to quench the galaxies and remove their gas content (e.g., Lin & Faber 1983; Boselli et al. 2008, 2014; Toloba et al. 2015), this may be a viable mechanism for the origins of UDGs. To test this scenario, more focused simulations are needed, in combination with further observational information (mainly to determine their total masses through robust stellar velocity dispersion measurements) about the UDG population. These models should also explain the presence of apparently isolated UDGs like DGSAT I. This would help to discriminate if these systems are tidally perturbed versions of a known type of galaxy or (as previously suggested) a new type of *peculiar dwarf* or *failed giant* depending upon their total masses (Beasley et al. 2016). DGSAT I could provide important leverage in discriminating between the models, owing to its presence at the outskirts—or beyond—of a galaxy cluster (Zw 0107+3212: with a projected distance of 1.8 Mpc). One possibility is that it is a "backsplash" galaxy that has passed through the center of the cluster (e.g., Gill et al. 2015).

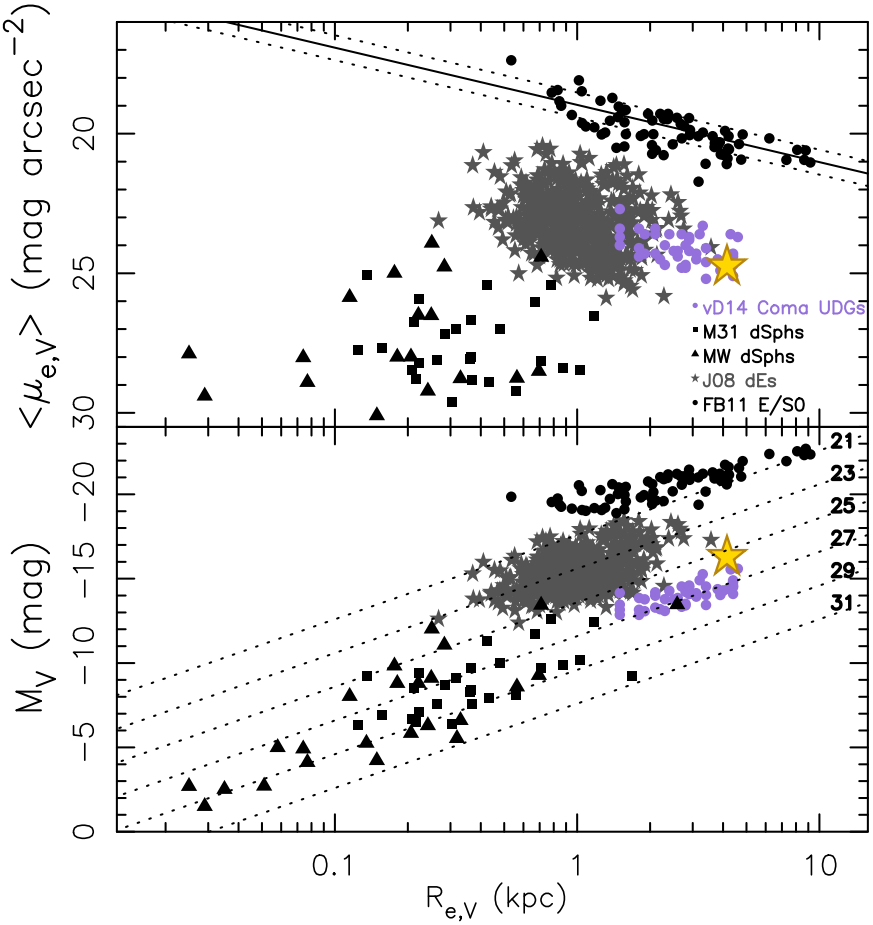

Figure 8. Scaling relations for early-type galaxies. Top panel: surface brightness vs. size in *V*-band relation adapted from Toloba et al. (2012). The black dots represent massive elliptical (E) and lenticular (S0) galaxies from Falcon-Barroso et al. (2011). The gray asterisks are Virgo dwarf early-types from Janz & Lisker (2008, 2009), the black triangles and squares are Milky Way and M31 dwarf spheroidal galaxies, respectively, from McConnachie (2012). The black solid and dotted lines are the best fit relation and $\pm 1\sigma$ scatter for the massive E/S0 galaxies from FB11. The yellow star indicate its position, assuming its likely membership in the Pisces-Perseus supercluster with a line of sight distance of 78 Mpc. Bottom panel: size–luminosity relation for early-type galaxies in the *V*-band. Symbols are as in the top panel. The dotted lines are lines of constant surface brightness. Their values in mag arcsec^{-2} are indicated at the right end of those lines.

Our detection of this hitherto unknown ultra-diffuse galaxy shows the value of using small aperture (10–15 cm) apochromatic telescopes with commercial CCD cameras to detect faint, low surface brightness galaxies which cannot be identified through resolved stellar populations or HI surveys. In fact, their wide fields and depths (2–3 mag deeper than the POSS-II survey) make them ideal for uncovering sparse areas of galaxy clusters up to 100 Mpc at low surface brightness levels, and check whether a significant population of still undetected, UDGs exist. These systems are still a mystery for modern galaxy formation scenarios, and could still remain undetected in large scale optical and radio surveys due to their extremely faint surface brightness and low gas content.

We thank the anonymous referee for helpful comments that improved the manuscript. We thank to Martha Haynes for kindly providing an update version of the Pisces-Perseus supercluster data from the ALFALFA survey plotted in Figure 5 and some useful comments. We also thank Thorsten Lisker and Joachim Janz for providing the Virgo dE catalogs and useful comments, Alan McConnachie for providing the broad-band VI photometry of the And II field for calibration, Sebastian Hidalgo for his help to compute the synthetic CMDs for the crowded simulations and Carlos Frenk and Till Sawala for useful comments. D.M.D. devotes this work to Ricardo González Rodríguez. D.M.D. was partly supported by an invited astronomer position at Observatoire de Paris (LERMA) in the initial phase of the project. D.M.D. and E.K.G. acknowledge support by Sonderforschungsbereich (SFB) 881 "The Milky Way System" of the German Research Foundation (DFB), particularly through subproject A2. T.S.C. acknowledges the support of a National Science Foundation Graduate Research Fellowship. The work in Russia is supported by the grant of the Russian Scientific Foundation 14-12-00965 and the RFBR grants 13-02-92690, 13-02-00780, and 15-52-45004. D.A.F. thanks the ARC for financial support via DP130100388. J.W. was supported by NSFC grant 11390372, 11373029 and 11261140641. This work was partially supported by the Spanish Ministerio de Economía y Competitividad (MINECO; grant AYA2010-21322-C03-02). E.T. acknowledges the financial support of the Fulbright Program jointly with the Spanish Ministry of Education. Based on data collected at Subaru Telescope (which is operated by the National Astronomical Observatory of Japan). We acknowledge the very significant cultural role and reverence that the summit of Mauna Kea has always had within the indigenous Hawaiian community. We are most fortunate to have the opportunity to conduct observations from this mountain.

REFERENCES

Abazajian, K. N., Adelman-McCarthy, J. K., Agüeros, M. A., et al. 2009, ApJS, 182, 543
Afanasiev, V. L., & Moiseev, A. V. 2005, AstL, 31, 194
Baba, H., Yasuda, N., Ichikawa, S.-I., et al. 2002, RNAOJ, 6, 23
Banse, K., Crane, P., Grosbol, P., et al. 1983, Msngr, 31, 26
Beasley, M., Romanowski, A., Pota, V., et al. 2016, ApJL, 819, L20
Bell, E. F., McIntosh, D. H., Katz, N., & Weinberg, M. D. 2003, ApJS, 149, 289
Bertin, E., & Arnouts, S. 1996, A&A, 117, 393
Binney, J., & Merrifield, M. 1998, Galactic Astronomy (Princeton, NJ: Princeton Univ. Press)
Blanton, M. R., Brinkmann, J., Csabai, I., et al. 2003, AJ, 125, 2348
Boselli, A., Boissier, S., Cortese, L., & Gavazzi, G. 2008, ApJ, 674, 742
Boselli, A., Voyer, E., Boissier, S., et al. 2014, A&A, 570, 69
Bothun, G., Impey, C., & McGaugh, S. 1997, PASP, 109, 745
Bovy, J., & Rix, H. W. 2013, ApJ, 779, 115
Caldwell, J. A. R. 2006, ApJ, 651, 822
Caldwell, J. A. R., Cousins, A. W. J., Ahlers, C. C., van Wamelen, P., & Maritz, E. J. 1993, SAAOC, 15, 1
Chen, Y., Girardi, L., Bressan, A., et al. 2014, MNRAS, 444, 2525
Conn, A. R., Lewis, G. F., Ibata, R. A., et al. 2011, ApJ, 740, 69
Conn, A. R., Ibata, R. A., Lewis, G. F., et al. 2012, ApJ, 758, 11
Cooper, A. P., Martínez-Delgado, D., Helly, J., et al. 2011, ApJL, 743, L21
Dohm-Palmer, R. C., Skillman, E. D., Saha, A., et al. 1997, AJ, 114, 2514
Falcon-Barroso, J., van de Ben, G., Peletier, R. F., et al. 2011, MNRAS, 417, 1787
Ferrarese, L., Coté, P., Cuillandre, J.-C., et al. 2012, ApJ, 200, 4
Gavazzi, G., Fumagalli, M., Cucciati, O., & Boselli, A. 2010, A&A, 517, 73
Geha, M., Blanton, M. R., Yan, R., & Tinker, J. L. 2012, ApJ, 757, 85
Geha, M., Guhathakurta, P., & van der Marel, R. P. 2003, AJ, 126, 1794
Gill, S. P. D., Knebe, A., & Gibson, B. K. 2015, MNRAS, 356, 1327
Giovanelli, R., & Haynes, M. P. 1989, AJ, 97, 633
Gnedin, A. 2003, ApJ, 589, 752
Ho, N., Geha, M., Muñoz, R. R., et al. 2012, ApJ, 758, 124
Impey, C., Bothun, G., & Malin, D. 1988, ApJ, 330, 634
Janz, J. R., & Lisker, T. 2008, ApJL, 689, L25
Janz, J. R., & Lisker, T. 2009, ApJL, 696, L102
Javanmardi, B., Martinez-Delgado, D., Kroupa, P., et al. 2015, A&A, submitted (arXiv:1511.04446)
Jordi, K., Grebel, E. K., & Ammon, K. 2006, A&A, 460, 339
Karachentsev, I. D., & Kaisina, E. I. 2013, AJ, 146, 46
Karachentsev, I. D., Riepe, P., Zilch, T., et al. 2015, AstBu, 70, 4
Kennicutt, R. C. 1998, ARA&A, 36, 189
Kim, S., Staveley-Smith, L., Dopita, M. A., et al. 1998, ApJ, 503, 674
Koda, J., Yagi, M., Yamanoi, H., & Komiyama, Y. 2015, ApJ, 807, 2
Koleva, M., Prugniel, P., Bouchard, A., & Wu, Y. 2009, A&A, n501, 1269
Koleva, M., Prugniel, P., Ocvirk, P., Le Borgne, D., & Soubiran, C. 2008, MNRAS, 385, 1998
Lang, D., Hogg, D. W., Mierle, K., Blanton, M., & Roweis, S. 2010, AJ, 139, 1782
Lin, D. N. C., & Faber, S. M. 1983, ApJL, 266, L21
Lisker, T., Grebel, E. K., & Binggeli, B. 2006, AJ, 132, 497
Martin, N. F., Ibata, R. A., McConnachie, A. W., et al. 2013, ApJ, 776, 80
Martínez-Delgado, D., Peñarrubia, J., Gabany, R. J., et al. 2008, ApJ, 689, 184
Martínez-Delgado, D., Gabany, R. J., Crawford, K., et al. 2010, AJ, 140, 962
Mastropietro, C., Moore, B., Mayer, L., Wadsley, J., & Stadel, J. 2005, MNRAS, 363, 509
Mayer, L., Governato, F., Colpi, M., et al. 2001, ApJ, 559, 754
McConnachie, A. W. 2012, AJ, 144, 4
McConnachie, A. W., Arimoto, N., & Irwin, M. 2007, MNRAS, 379, 379
McConnachie, A. W., Huxor, A., Martin, N., et al. 2008, ApJ, 688, 1009
McConnachie, A. W., Irwin, M. J., Ibata, R. A., et al. 2009, Natur, 461, 66
Merritt, A., van Dokkum, P., & Abraham, R. 2014, ApJ, 787, 37
Mihos, J. C., Durrell, P. R., Ferrarese, L., et al. 2015, ApJL, 809, L21
Miyazaki, S., Komiyama, Y., Sekiguchi, M., et al. 2002, PASJ, 54, 833
Moore, B., Ghigna, S., Governato, F., et al. 1999, ApJ, 524, 19
Moore, B., Lake, G., & Katz, N. 1998, ApJ, 495, 139
Muñoz, R. P., Eigenthaler, P., Puzia, T. H., et al. 2015, ApJL, 813, L15
Peng, C. Y., Ho, L. C., Impey, C. D., & Rix, H. W. 2010, AJ, 139, 2097
Romanowsky, A. J., Martínez-Delgado, D., Martin, N. F., et al. 2016, MNRAS, 457, L103
Salpeter, E. E. 1955, ApJ, 121, 161
Sanchez-Blazquez, P., Peletier, R. F., Jimenez-Vicente, J., et al. 2006, MNRAS, 371, 703
Schlegel, D. J., Finkbeiner, D. P., & Davis, M. 1998, ApJ, 500, 525
Stetson, P. 1987, PASP, 99, 191
Tody, D. 1993, in ASP Conf. Ser. 52, Astronomical Data Analysis Software and Systems II, ed. R. J Hanisch, R. J. V. Brissenden, & J. Barnes (San Francisco, CA: ASP), 173
Toloba, E., Boselli, A., Peletier, R. F., et al. 2012, A&A, 548, A78
Toloba, E., Guhathakurta, P., Boselli, A., et al. 2015, ApJ, 799, 172
Toloba, E., Guhathakurta, P., Peletier, R. F., et al. 2014, ApJS, 215, 17
Tonry, J., & Davis, M. 1979, AJ, 84, 1511
Tully, R. B., Shaya, E. J., Karachentsev, I. D., et al. 2008, ApJ, 676, 184
van Dokkum, P. G., Abraham, R., Merritt, A., et al. 2015a, ApJ, 798, 45
van Dokkum, P. G., Romanowsky, A. J., Abraham, R., et al. 2015b, ApJL, 804, L26
Vazdekis, A., Sanchez-Blazquez, P., Falcon-Barroso, J., et al. 2010, MNRAS, 404, 1639
Wegner, G., Haynes, M. P., & Giovanelli, R. 1993, AJ, 105, 1251
Williams, B. F., Dalcanton, J. J., Gilbert, K. M., et al. 2010, ApJ, 716, 71
Zibetti, S., Charlot, S., & Rix, H.-W. 2010, MNRAS, 400, 1181